Global and Planetary Change 82–83 (2012) 65–73

Contents lists available at SciVerse ScienceDirect

Global and Planetary Change

journal homepage: www.elsevier.com/locate/gloplacha

# Spatially downscaling GCMs outputs to project changes in extreme precipitation and temperature events on the Loess Plateau of China during the 21st Century

Zhi Li [a,b,*], Fen-Li Zheng [c], Wen-Zhao Liu [c], De-Juan Jiang [d]

[a] College of Resources and Environment, Northwest A & F University, Yangling, 712100, Shaanxi, China
[b] Institute of Water Saving Agriculture in Arid Areas of China, Northwest A&F University, Yangling, 712100, Shaanxi, China
[c] Institute of Soil and Water Conservation, CAS & MWR, Yangling, 712100, Shaanxi, China
[d] Yantai Institute of Coastal Zone Research, Chinese Academy of Sciences, Yantai, 264003, China

ARTICLE INFO

*Article history:*
Received 1 December 2010
Accepted 15 November 2011
Available online 23 November 2011

*Keywords:*
climate change
extreme temperature events
Loess Plateau
spatial downscaling

ABSTRACT

A simple transfer function method is used to spatially downscale extreme precipitation and temperature indices of six GCMs (CNRM-CM3, GFDL-CM2.1, INM-CM3.0, IPSL-CM4, MIROC3.2_M and NCAR-PCM) under three emission scenarios (A1B, A2, B1) from grid outputs to target station to project their potential spatio-temporal changes on the Loess Plateau of China during the 21st century. GCMs project that extreme climate events will keep the present change trend, i.e. longer heatwave duration and growing season length, less cold extremes, smaller annual extreme temperature range, more frequent and intense precipitation, and longer drought duration; and climate models suggest that the changes during the 21st century are a further amplification of those at present. Spatial variations exist in the changes of extreme indices, the greatest changes will occur in the southeast and northwest region for extreme precipitation indices while in the north and southeast region for extreme temperature events. The projected changes in extreme climate will possibly bring great impacts on the soil losses and agriculture on the Loess Plateau and countermeasures should be planned.



## 1. Introduction

Since extreme climate events are likely to cause more damages to society and ecosystems than simple shifts in the mean values (Katz and Brown, 1992; Mearns et al., 1997), increasing concerns about their changes arise. A variety of studies have analyzed the change trends of historical extreme climate events in different areas of the world (Frich et al., 2002; Wang and Zhou, 2005; Alexander et al., 2006; Bocheva et al., 2009), and some significant trends have been detected, such as increases in the number of daily warm extremes and reductions in the number of daily cold extremes, and increases in heavy precipitation events and droughts (IPCC, 2007). As extreme climate events have great adverse impacts to a large extent, their change trends in the future should be paid more attention; therefore, some useful information can be provided for developing climate change mitigation and adaptation strategies.

To quantify the changes of extreme climate events, ten indices (five temperature-based and five precipitation-based indices) proposed by Frich et al. (2002) have been selected by ten General Circulation Models (GCMs) in support of the IPCC AR4 to simulate past changes and project future changes of extreme climate events. Though these results provide important information, some work still need to be done to get more accurate projections due to the coarse resolutions of GCMs (grid outputs, Table 1). For example, a similar study conducted in the Yangtze River Basin finds that six GCMs all overestimate extreme indices and don't reproduce the spatial pattern well (Xu et al., 2009). Therefore, it is important to downscale the GCMs grid outputs to local scale. To downscale GCMs outputs, two kinds of methods are often used, i.e. dynamic and statistical methods (IPCC, 2001). The dynamic methods, namely regional climate modeling (RCM), can generate higher resolution data and is often used in extreme climate events study (Goubanova and Li, 2007; Kyselý and Beranová, 2008; Fischer and Schär, 2009; Coppola and Giorgi, 2010; Im et al., 2011); however, RCM is time-consuming and costly. Statistical methods are easy to realize and can be calibrated to local conditions, which is widely used in extreme climate projection in recent years (Wilby et al., 1998; Katz, 1999; Zhang, 2005; Li et al., 2011; Taye et al., 2011).

Future changes in extreme climate events have been discussed over many regions. In general, great spatiotemporal variations exist in the potential changes of extreme precipitation events (EPE). However, extreme temperature events (ETE) have more significant responses to global warming than EPE and coherent spatial patterns of significant changes in ETE have been detected, such as longer heatwave duration, less cold nights, smaller annual extreme temperature range (Alexander et al., 2006; IPCC, 2007). It should be noted that the

* Corresponding author at: College of Resources and Environment, Northwest A & F University, Yangling, 712100, Shaanxi, China.
*E-mail address:* lizhibox@126.com (Z. Li).

0921-8181/$ – see front matter © 2011 Elsevier B.V. All rights reserved.
doi:10.1016/j.gloplacha.2011.11.008

**Table 1**
The indices of extreme climate events.

| Indices | Name | Definition | Unit |
|---|---|---|---|
| CDD | Consecutive dry days | Maximum number of consecutive days with PRCP<1 mm | day |
| R10 | Number of heavy precipitation | Annual count of days when PRCP>10 mm | day |
| R5d | Max 5 days precipitation amount | Monthly maximum 5-day precipitation | mm |
| R95t | Annual rainfall fraction due to very wet days | Fraction of annual total precipitation due to events exceeding the 95th percentile of the 1961–1990 base period | % |
| SDII | Simple daily intensity index | Annual total precipitation divided by the number of wet days (defined as PRCP>1.0 mm) in the year | mm/day |
| TN90 | Warm nights | Percent of time Tmin>the long-term 90th percentile value of daily Tmin | % |
| FD | Total number of frost days | Days with Tmin<0 °C | day |
| ETR | Intra-annual extreme temperature range | Difference between the highest and the lowest temperature of the same calendar year | °C |
| GSL | Growing season length | Period between when Tday>5 °C for>5 d and Tday<5 °C for>5 d | day |
| HWDI | Heat wave duration index | Maximum period>5 consecutive days with Tmax>5 °C above the 1960–1990 daily Tmax normal | day |

projected results are also subject to the uncertainties due to GCMs, downscaling methods, and regions (Olesen et al., 2007; Kay et al., 2009; Prudhomme and Davies, 2009). Therefore, assessing changes of extreme climate events should be carried out in different regions using multi-GCMs under multi-emission scenarios with different methods to obtain more accurate results.

The Loess Plateau is situated in the middle reaches of the Yellow River basin, north China (Fig. 1). Most areas of the Loess Plateau belong to sub-humid and semi-arid climate with average annual precipitation ranging from 200 mm in the northwest to 750 mm in the southeast. The rainy season from June to September accounts for 60-70% of the total precipitation, most of which is in the form of high intensity rainstorms (Zhang et al., 2008; Li et al., 2009). The rainstorms contribute greatly to the soil and water losses in the Loess Plateau. Though only about 6% rainfall generate runoff, soil losses caused by one severe heavy storm can account for 60-90% of the annual soil losses (Zhou and Wang, 1992). The combined effects of frequent heavy rainfall, steeply sloping landscapes, low vegetation cover, and highly erodible soils have ranked the Loess Plateau as one of the most severely eroded areas in the world, with an estimated mean annual soil loss rate of 5,000-10,000 tonnes $km^{-2}$ $year^{-1}$ (Zhang et al., 2008). Rain-fed farming systems account for 80% of the total cultivated land area on the Loess Plateau (Shan, 1994), and the agriculture is greatly dependent on and sensitive to climate (Wang and Liu, 2003). As extreme temperature events can affect crop growth differently with changes in frequency versus continuous days of maximum versus minimum temperature, a short period of abnormally high or low temperatures can cause significant damage to crop growth and final yield (Thompson, 1975; Mearns et al., 1984). For example, a heavy frost hitting Ningxia Province on the Loess Plateau from May 3 to May 4 in 2004, affected the growth of crops in an area of 312823 $hm^2$, and caused direct economic loss of 0.65 billion CNY (about 0.1 billion U.S. dollars) (Yang et al., 2008).

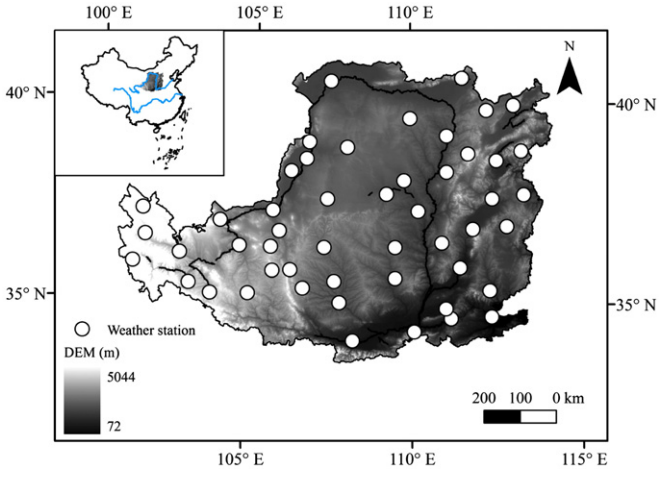


**Fig. 1.** Location of the Loess Plateau and its meteorological stations.

Environmental changes have been detected in recent years on the Loess Plateau. For example, runoff and sediment from the Loess Plateau to the Yellow River have decreased significantly in recent decades. Some studies reveal that climate changes play an important role (Li et al., 2007; Li et al., 2009) as the annual precipitation decreases slightly while the mean annual temperature and pan evaporation increase significantly (Xu et al., 2007). These previous studies focused on the mean values can partially interpret the environmental changes; however, as stated above, more attention should be paid on extreme climate as they are the main reasons causing soil erosion and agricultural disasters.

Our previous research shows that EPE on the Loess Plateau have not changed significantly; however, ETE has significant change, for example, hot-day threshold, cold-night threshold, and the longest heatwave duration tend to increase while the number of frost days decreases during 1961–2007 (Li et al., 2010). Under the background of global change, how will the extreme climate events change in the future? This is of great importance for the soil loss control and agriculture in this region. The objective of this study is to project the spatial and temporal changes of extreme precipitation and temperature events on the Loess Plateau during the 21st century.

## 2. Data and Methods

### 2.1. Data description

Ten extreme climate indices developed by Frich et al. (2002) and subsequently adopted by the Intergovernmental Panel on Climate Change (IPCC) are used to quantify the extreme climate events (Table 1). Five indices are used to describe the frequency (CDD, R10) and intensity (R5d, R95t and SDII) of EPE while the other five indices are used to quantify the frequency (TN90 and FD) and intensity (ETR, GSL and HWDI) of ETE. Extreme indices during 1961–2007 and 2011–2099 are both necessary for GCM statistical downscaling to project potential changes in extreme climate.

Historical extreme indices during 1961–2007 are calculated using daily data from 48 weather stations (Fig. 1) distributed evenly on the Loess Plateau. The historical daily data include precipitation, maximum, minimum and mean temperature, which are provided by China Meteorological Administration and have been carried out quality control.

Simulated extreme indices are provided by six GCMs (CNRM_CM3, GFDL_CM2.1, INMCM3.0, IPSL_CM4, MIROC3.2_M and NCAR_PCM1) on an annual basis from the CMIP3 (Coupled Model Intercomparison

**Table 2**
The GCMs and emission scenarios used in this study.

| GCMs | Country | Resolution | Data duration | | | |
|---|---|---|---|---|---|---|
| | | | 20C3M | A2 | A1B | B1 |
| CNRM-CM3 | France | 128×64 T42 | 1860-1999 | 2000-2099 | 2000-2299 | 2000-2299 |
| GFDL-CM2.1 | USA | 144×90 L24 | 1861-2000 | 2001-2100 | 2001-2300 | 2001-2300 |
| INM-CM3.0 | Russia | 72×45 L21 | 1871-2000 | 2001-2200 | 2001-2200 | 2001-2200 |
| IPSL-CM4 | France | 96×72 L19 | 1860-2000 | 2000-2100 | 2000-2230 | 2000-2300 |
| MIROC3.2_M | Japan | 128×64 T42L20 | 1850-2000 | 2001-2100 | 2001-2100 | 2001-2100 |
| NCAR-PCM | USA | 128×64 T42L26 | 1890-1999 | 2000-2099 | 2000-2099 | 2000-2099 |

Project phase 3) for both hindcasted and projected periods (Table 2). These models are used because they provide detailed extreme indices and some of them have been proved to perform well in simulating the surface air temperature over China (Zhou and Yu, 2006; Xu et al., 2009). To carry out statistical spatial downscaling, two kinds of emission scenarios are used, i.e. historical and future emission scenarios. 20C3M is a kind of historical emission scenario running with greenhouse gasses increasing as observed through the 20th century, and it will be used to develop regression equation with the historical data. Three future emission scenarios, i.e. B1, A1B and A2, are selected to project the climate changes under the low, middle and high emission rates of greenhouse gases, in which $CO_2$ concentration will be about 550, 700 and 850 ppm by 2100, respectively. The periods of 1961–1999 and 2011–2099 are used in this study, which will be described detailed in the following parts.

As the ten extreme indices are provided by GCMs on an annual basis, the observed indices are also calculated at annual time scales. Therefore, the following operations such as developing transfer functions and projecting future changes are all based on an annual time scale.

### 2.2. Spatial downscaling

A simple transfer function developed through quartile plots is used to spatially downscale GCMs gird outputs to target station. The quartile plots, i.e. QQ-plots, pair the measured and GCMs-hindcasted annual extreme indices by their ranks or corresponding quartiles. The best fitting function to each plot is the transfer function. Two kinds of equations, i.e. a simple univariate linear and a nonlinear function, are developed as transfer functions between two sets of data for each extreme index during 1961–1999. The period 1961–1999 is selected because the simulated periods of GCMs under 20C3M scenario are different, for example, CNRM-CM3 and NCAR-PCM hindcast data to 1999 while the simulations of the other GCMs are up to 2000 (Table 2).

The transfer function is then applied to GCMs grid outputs for three 30-year time slices, i.e. 2020s (2011–2040), 2050s (2041–2070) and 2080s (2071–2099), to carry out spatial downscaling. The nonlinear function is used to transform the GCMs indices that are within the range in which the nonlinear function is fitted, while the linear function is used for the values outside the range. The use of linear functions for the out-of-range values is to generate conservative, first-order approximations. The downscaled extreme indices are used to calculate mean of the changed climate for the period. This procedure is repeated for each extreme index at each station. Readers are referred to Zhang (2005) and Li et al. (2011) for more detailed description of the method.

### 2.3. Spatial interpolation and temporal changes analysis

The Inverse Distance Weighted (IDW) interpolation method is used to generate the spatial distribution of the extreme indices. For the future changes in spatial pattern, we focus mainly on the end of the 21st century (2071–2099) for brevity, the differences between the mean historical values during 1961–2007 and downscaled multi-model ensemble mean for the ten indices during 2071–2099 are interpolated to show the future changes.

As the spatial downscaling methods used in this study cannot generate time series of future extreme indices, the temporal changes of future extreme indices are quantified by downscaled multi-model ensemble means of three 30-year time slices, i.e. 2020s, 2050s and 2080s. Independent one-sample *t*-test is used to quantify the significance of future changes compared with present (1961–2007), and the confidence level is 95%.

## 3. Results

### 3.1. Temporal changes of extreme precipitation indices during the 21st century

Table 3 shows the ensemble mean of extreme precipitation indices from six GCMs under three emission scenarios during 2020s, 2050s and 2080s and their relative changes compared with 1961–2007. It is easy to judge the change trend of each index, i.e. CDD will keep decreasing while the other four indices will increase during the 21st century. The change magnitude of each index increases over time, and the greatest changes will occur during 2080s. A preliminary conclusion can be drawn, i.e. EPE during the 21st century will possibly be more frequent and intense and the changes at the end of the 21st century are a further amplification of those at present and in the middle of the century (Li et al., 2010).

### 3.2. Spatial variations in the changes of extreme precipitation indices

The spatial patterns of EPE in the 21st century will be similar as the present (Li et al., 2010); however, spatial variations exist in the projected changes during the 21st century. 2080s is only taken as an example to interpret this aspect for brevity (Fig. 2). CDD will decrease in the northwest region with maxima of 18 days and the magnitudes increase from southeast to northwest; meanwhile, CDD will increase in the southeast region with maxima of five days. The other four indices will all increase over the Loess Plateau; specifically, R10, R5d, R95t and SDII will increase by 0.8-5.9 days, 5.8-29.7 mm, 1.6-9.2% and 0.5-1.7 mm/day, respectively. However, the greatest increase in each index occurs in different region. R10 has the greatest increase in the southwest and northeast region; R5d and SDII both

**Table 3**
The projected changes of extreme precipitation indices averaged across six GCMs under three emission scenarios during 2011-2099.

| Period | 1961-2007 | 2011-2040 | | 2041-2070 | | 2071-2099 | |
|---|---|---|---|---|---|---|---|
| | Mean | Mean | Change | Mean | Change | Mean | Change |
| CDD, day | 57.5 | 56.7 | −0.8 | 55.4 | −2.1 | 54.1 | −3.5 |
| R10, day | 12.9 | 13.6 | 0.6 | 14.4 | 1.5 | 15.0 | 2.0 |
| R5d, mm | 73.2 | 79.2 | 6.0 | 84.5 | 11.3 | 89.7 | 16.4 |
| R95t, % | 25.8 | 27.6 | 1.8 | 28.5 | 2.6 | 29.9 | 4.0 |
| SDII, mm/day | 7.9 | 8.2 | 0.3 | 8.6 | 0.8 | 9.0 | 1.2 |

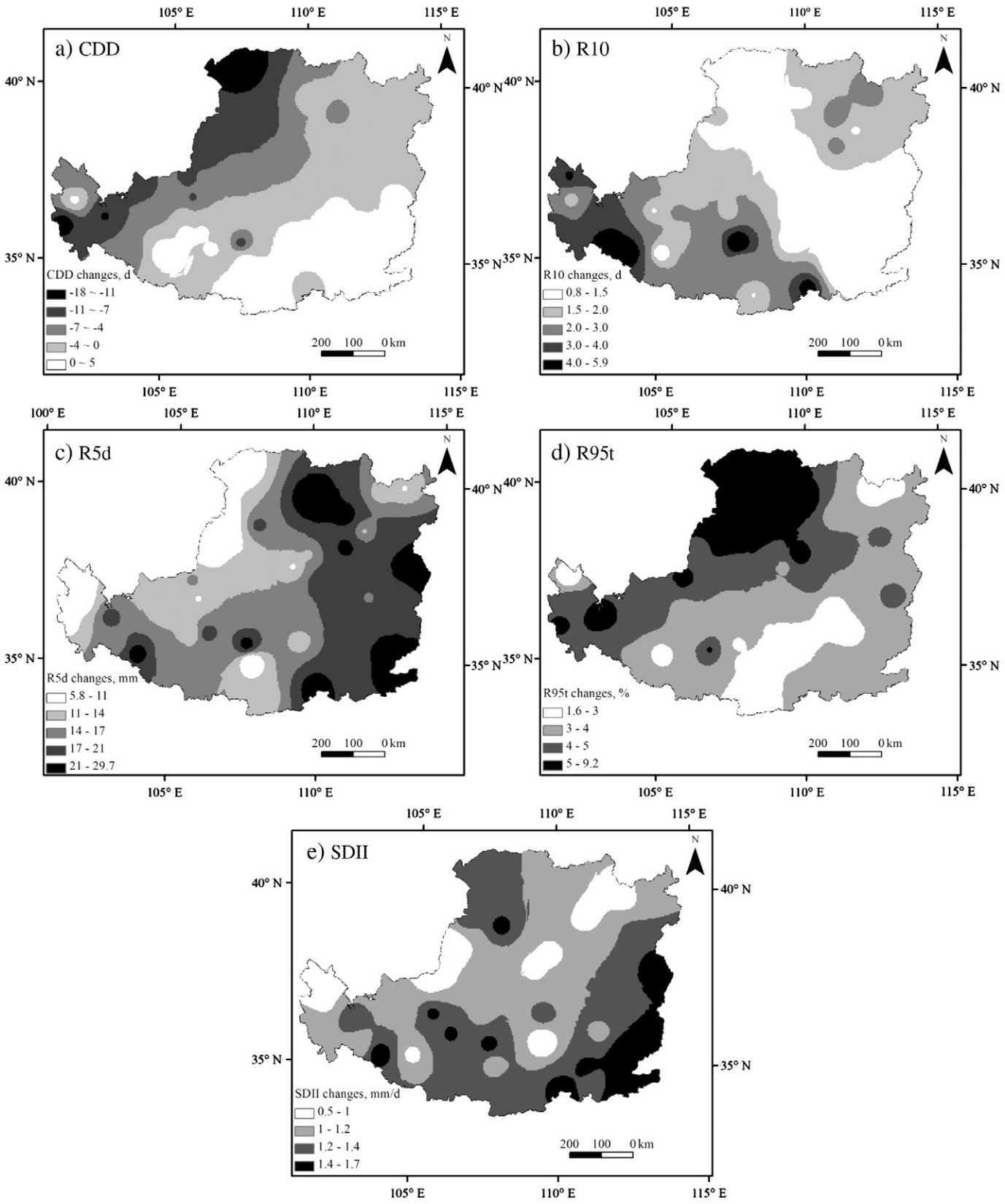


**Fig. 2.** Spatial patterns of changes in extreme precipitation indices during 2071–2099 compared with 1961–2007.

increase pronounced in the east or southeast region; R95t increases the most in northwest region. Overall, the projected changes tend to increase or decrease the spatial variation in EPE. For example, changes in CDD will lead to a more homogenous spatial pattern for drought on the Loess Plateau in the future as CDD increase from southeast to northwest at present (Li et al., 2010). However, changes in R5d, R95t and SDII will increase their spatial variation as the spatial patterns of projected changes are consistent with the present spatial

**Table 4**
The projected changes of extreme temperature indices averaged across six GCMs under three emission scenarios during the 21st century.

| Period | 1961-2007 | 2011-2040 | | 2041-2070 | | 2071-2099 | |
|---|---|---|---|---|---|---|---|
| | Mean | Mean | Change | Mean | Change | Mean | Change |
| TN90, % | 16 | 18 | 2 | 20 | 4 | 22 | 6 |
| FD, days | 149 | 139 | −10 | 129 | −20 | 120 | −29 |
| ETR, °C | 56.5 | 56.5 | 0 | 55.8 | −0.7 | 55.3 | −1.2 |
| GSL, days | 221 | 230 | 9 | 238 | 17 | 245 | 24 |
| HWDI, days | 8 | 16 | 8 | 28 | 20 | 49 | 41 |

distribution. Over all, the frequency and intensity of extreme precipitation events at the end of the 21st century will increase based on present spatial distribution, and the greatest changes will possibly occur in the southeast and northwest regions.

### 3.3. Temporal changes in the extreme temperature indices during the 21st century

Compared with 1961–2007, TN90, GSL and HWDI will increase while FD and ETR will decrease during the 21st century (Table 4), which is consistent with the present change trend on the Loess Plateau (Li et al., 2010) and other regions in the world (Alexander et al., 2006; IPCC, 2007). The absolute change magnitudes of each index increase with time, the change magnitudes during 2020s are the smallest while those during 2080s are the biggest with the moderate value during 2050s, which implies that the change trend of temperature-based indices will be stable during the 21st century. During 2020s, averaged across all GCMs, TN90, GSL and HWDI will increase by 2%, 9 days and 10 days, respectively; FD and ETR will decrease by 0.4 °C and 10 days, respectively. The change magnitudes of TN90, FD, ETR and GSL during 2050s and 2080s are about twice or three times of those during 2020s, respectively. For example, TN90 and GSL will increase by 2% and 8 days for each period and reach the increase magnitude of 6% and 24 days at the end of the 21st century, respectively; FD and ETR will decrease by 10 days and 0.5 °C for each 30 years and reduce 29 days and 1.6 °C at the end of the 21st century, respectively. However, the change magnitudes of HWDI during the latter period are almost twice of those during the former period. The increase magnitudes during three periods are 10, 22 and 43 days, respectively. The great increase speed of HWDI implies that heat wave duration will be much longer and its impacts on natural system will be more serious in the future.

### 3.4. Spatial variations in the changes of extreme temperature indices

The mean projected changes in extreme temperature indices during 2071–2099 are also interpolated as an example to interpret the spatial variations (Fig. 3). Though wide ranges are detected in the projected changes, one or two dominant change ranges for each extreme temperature index cover most areas on the Loess Plateau. One dominant change range is detected for TN90, ETR and GSL. For example, the change ranges of TN90, ETR and GSL are 0.4 to 11.5%, -11.7 to 6.8 °C and 7.5 to 60.4 days, respectively; however, 5 to 7%, less than 2 °C and 20 to 30 days are the dominant change ranges for them, respectively. For FD and HWDI, the situation is more complicated. Two dominant changes exist in FD, and FD will decrease by 20–30 days in the southeastern region while decrease by 30–40 days in the northwestern region. The increase of HWDI shows a ring distribution and is incremental from the border to the center, and the highest increase is 55–62 days. Though the dominant changes are different for each index, extreme temperature events will have the greatest changes over the north and southwest regions on the Loess Plateau at the end of the 21st century.

## 4. Discussion

### 4.1. Multiple models and emission scenarios

Obvious uncertainties exist in future projection of extreme climate indices among models or scenarios, and the uncertainties increase when projecting extreme indices for a more distant future.

The projected change trend in extreme precipitation indices is similar among different GCMs and ES, i.e. heavy rainfall will be more frequent and intense while drought duration will be longer; however, the change magnitudes and stations with significant changes detected by T-test are quite different (Fig. 4). Changes in CDD vary from −5.2 to 5.9 days during 2020s and from −9.7 to 1.7 days during 2080s. Most scenarios project CDD will decrease, however, the stations with significant trend vary greatly for different scenarios. For example, the numbers of stations with significant trend during 2020s and 2050s are less than 10 for most scenarios, while the numbers during 2080s are more than 10 for most scenarios. The variations in change magnitude and numbers of stations with significant trend for CDD are relatively conservative; however, larger variations exist in the other indices. Taking R5d as an example, its changes vary from 0.9 to 12.7 mm during 2020s and from 3.0 to 35.0 mm in 2080s; the numbers of stations with significant trend during 2020s are all less than 20 while those during 2050s and 2080s both range from 0 to 50.

As for the extreme temperature indices, the projected changes are insensitive to GCM or emission scenarios for TN90, FD, ETR and GSL (Table 5). The coefficients of variation are all less than 0.1 for GCMs or emission scenarios during each period, which means the variation is relatively low. However, HWDI is more sensitive to GCMs or emission scenarios as the coefficients of variation are all greater than 0.1 for the three periods. It should be noted that the variation of extreme indices for GCMs or emission scenarios increases with time, the coefficients of variation of extreme temperature indices during 2050s are greater than those during 2020s, and the situation is similar for the period of 2050s and 2080s. GCMs project more consistent results for the near future while uncertainties increase with time. The coefficients of variation for projected extreme indices are less than those in raw GCMs outputs, which implies that the downscaling method reduce the uncertainties due to multi-models effectively.

Overall, uncertainty in the projections due to multiple models and emission scenarios is less for ETE than EPE characterized by smaller coefficients of variation in ETE indices and a larger dispersion on the EPE scatter plots (Fig. 4). For each extreme index, uncertainties increase with time as shown by the increase in scatter in Fig. 4 and the coefficient of variation in Table 5. It should be noted that uncertainty due to GCMs is greater than that linked with emission scenarios as the points of different emission scenarios from the same GCMs are often staying together, and this is particularly obvious during 2080s (Fig. 4). IPSL projects the most changes while GFDL has the least changes for most indices, and A2 projects the most changes while B1 projects the least changes; therefore, any climate change study based on only one GCMs or emission scenario should be cautious.

### 4.2. The impacts of extreme climate events on environment

According to some researches, the soil loss reduction in recent years on the Loess Plateau is mainly due to the increasing vegetation cover and engineering measures (Li et al., 2007; Mu et al., 2007; Lin et al., 2009). However, it should be noted that this is possibly only true based on the fact that frequency and intensity of EPE change insignificantly and even decrease (Li et al., 2010). As mentioned above, annual soil losses on the Loess Plateau is only caused by several storms (Zhou and Wang, 1992), and intense heavy rainfall is the most important reason for the soil erosion regardless of vegetation in many

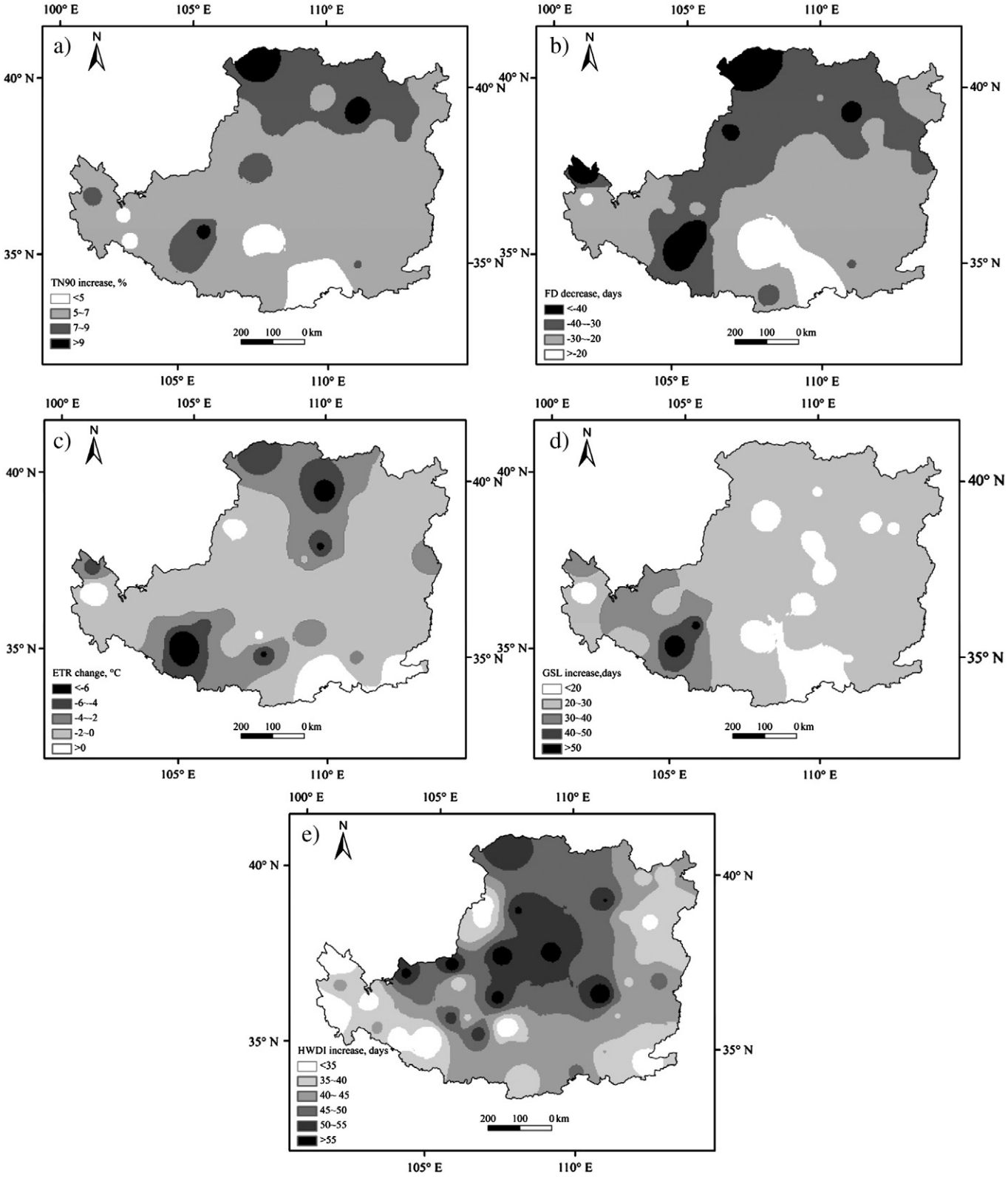


**Fig. 3.** The spatial pattern of mean projected changes in extreme temperature indices during 2071–2099.

regions (Xu, 2004). Therefore, the situation might be greatly different if the present EPE have an opposite change trend. Therefore, the change trend in EPE during the 21st century, i.e. to be more intense and frequent, will possibly exacerbate the water and soil losses on the Loess Plateau. Caution should be paid to these potential impacts and countermeasures should be taken in advance.

## 5. Conclusion

Frequent and intense rainstorms are one of the most important reasons for the severe soil losses while extreme temperature events are the main sources of agricultural disasters on the Loess Plateau; therefore, it is very important to project the future changes in the

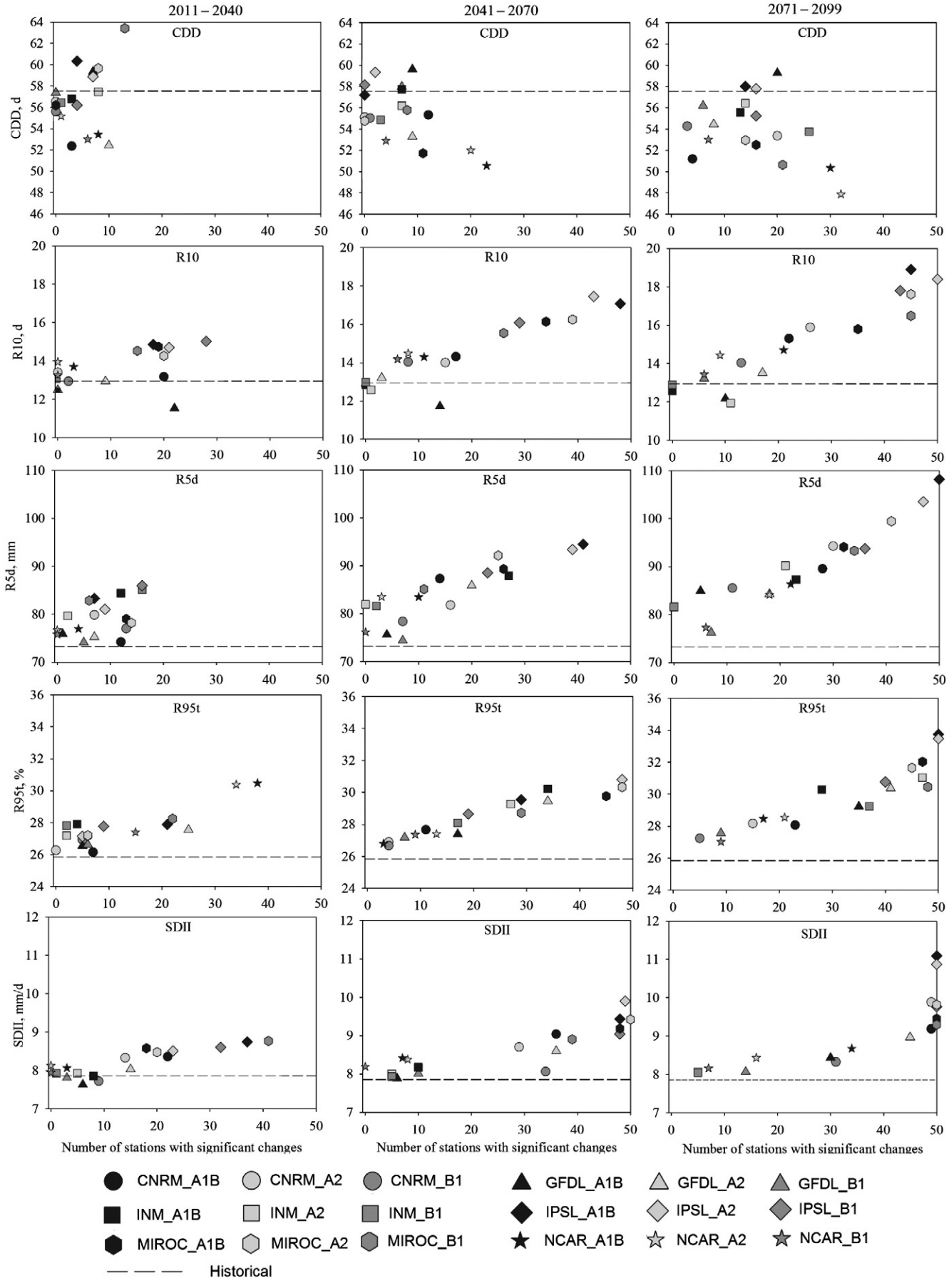


**Fig. 4.** Projected changes and numbers of stations with significant trend on the Loess Plateau in the 21st century using six GCM under three emission scenarios.

**Table 5**
Projected extreme temperature indices during the 21st century for multi-GCMs and multi-emission scenarios.

| | 2011-2040 | | | | | 2041-2070 | | | | | 2071-2099 | | | | |
|---|---|---|---|---|---|---|---|---|---|---|---|---|---|---|---|
| | TN90 | FD | ETR | GSL | HWDI | TN90 | FD | ETR | GSL | HWDI | TN90 | FD | ETR | GSL | HWDI |
| CNRM-CM3 | 18 | 138 | 56 | 231 | 21 | 20 | 129 | 54 | 239 | 31 | 22 | 119 | 52 | 250 | 49 |
| GFDL-CM2.1 | 18 | 142 | 57 | 225 | 14 | 19 | 130 | 56 | 234 | 28 | 22 | 119 | 58 | 240 | 42 |
| INM-CM3.0 | 18 | 138 | 59 | 230 | 16 | 19 | 132 | 58 | 236 | 19 | 21 | 125 | 57 | 244 | 28 |
| IPSL-CM4 | 18 | 139 | 56 | 232 | 12 | 21 | 129 | 57 | 240 | 28 | 24 | 118 | 58 | 251 | 57 |
| MIROC3.2_M | 19 | 136 | 55 | 231 | 19 | 22 | 123 | 54 | 242 | 49 | 25 | 111 | 52 | 246 | 97 |
| NCAR-PCM | 18 | 139 | 56 | 231 | 13 | 19 | 133 | 56 | 236 | 17 | 21 | 128 | 55 | 241 | 20 |
| C.V. | 0.02 | 0.01 | 0.03 | 0.01 | 0.23 | 0.05 | 0.02 | 0.03 | 0.01 | 0.40 | 0.08 | 0.05 | 0.05 | 0.02 | 0.56 |
| A1B | 18 | 137 | 56 | 232 | 16 | 21 | 126 | 55 | 241 | 32 | 23 | 116 | 55 | 249 | 56 |
| A2 | 18 | 140 | 57 | 227 | 14 | 20 | 129 | 56 | 236 | 29 | 24 | 115 | 55 | 249 | 59 |
| B1 | 18 | 138 | 56 | 231 | 18 | 19 | 133 | 56 | 235 | 24 | 20 | 128 | 55 | 239 | 31 |
| C.V. | 0.01 | 0.01 | 0.01 | 0.01 | 0.12 | 0.04 | 0.03 | 0.01 | 0.01 | 0.15 | 0.08 | 0.06 | 0.00 | 0.02 | 0.32 |

C.V., Coefficients of Variation.

extreme climate events in this region. Ten extreme climate indices from six GCMs (CNRM-CM3, GFDL-CM2.1, INM-CM3.0, IPSL-CM4, MIROC3.2_M and NCAR-PCM) under three emission scenarios (A1B, A2, B1) are spatially downscaled to estimate the potential changes of extreme precipitation and temperature events during the 21st century. GCMs project that the present change trend of extreme climate will continue during the 21st century, i.e. longer heatwave duration and growing season length, less cold extremes, smaller annual extreme temperature range, more frequent and intense precipitation, and longer drought duration. The absolute change magnitudes of each index increase with time, the changes during the 21st century are a further amplification of those at present. Spatial variations exist in the changes of extreme indices. Climate models suggest that the greatest changes will occur in the southeast and northwest region for extreme precipitation indices while in the north and southeast region for extreme temperature events at the end of the 21st century. Extreme temperature indices have more consistent spatial patterns than extreme precipitation indices. Overall, the projected changes in extreme climate events will possibly bring some adverse impacts to the soil losses and agriculture on the Loess Plateau, countermeasures should be planned in advance.

## Acknowledgements

This study is funded by the National Natural Science Foundation of China (No.41101022 & No.51179161) and the National Science & Technology Supporting Plan (No.2006BAD09B09). The authors are grateful to the National Climatic Centre (NCC) of the China Meteorological Administration (CMA) and the modeling groups, the Program for Climate Model Diagnosis and Intercomparison (PCMDI) and the WCRP's Working Group on Coupled Modeling (WGCM) for providing the data. We greatly appreciate the constructive suggestions from two anonymous referees.

## References

Alexander, L.V., Zhang, X., Peterson, T.C., Caesar, J., Gleason, B., Klein Tank, A.M.G., Haylock, M., Collins, D., Trewin, B., Rahimzadeh, F., Tagipour, A., Rupa Kumar, K., Revadekar, J., Griffiths, G., Vincent, L., Stephenson, D.B., Burn, J., Aguilar, E., Brunet, M., Taylor, M., New, M., Zhai, P., Rusticucci, M., Vazquez-Aguirre, J.L., 2006. Global observed changes in daily climate extremes of temperature and precipitation. Journal of Geophysical Research 111. doi:10.1029/2005JD006290.

Bocheva, L., Marinova, T., Simeonov, P., Gospodinov, I., 2009. Variability and trends of extreme precipitation events over Bulgaria (1961–2005). Atmospheric Research 93, 490–497.

Coppola, E., Giorgi, F., 2010. An assessment of temperature and precipitation change projections over Italy from recent global and regional climate model simulations. International Journal of Climatology 30, 11–32.

Fischer, E., Schär, C., 2009. Future changes in daily summer temperature variability: driving processes and role for temperature extremes. Climate Dynamics 33, 917–935.

Frich, P., Alexander, L.V., Della-Marta, P., Gleason, B., Haylock, M., Klein Tank, A.M.G., Peterson, T., 2002. Observed coherent changes in climatic extremes during the second half of the twentieth century. Climate Research 19, 193–212.

Goubanova, K., Li, L., 2007. Extremes in temperature and precipitation around the Mediterranean basin in an ensemble of future climate scenario simulations. Global and Planetary Change 57, 27–42.

Im, E.S., Jung, I.W., Bae, D.H., 2011. The temporal and spatial structures of recent and future trends in extreme indices over Korea from a regional climate projection. International Journal of Climatology 31, 72–86.

IPCC, 2001. Climate Change 2001: Impact, Adaptation and Vulnerability. Contribution of Working Group II to the Third Assessment Report of the Intergovernmental Panel on Climate Change. Cambridge University Press, Cambridge, UK.

IPCC, 2007. Climate Change 2007: The Physical Science Basis. Contribution of Working Group I to the Fourth Assessment Report of the Intergovernmental Panel on Climate Change. Cambridge University Press, Cambridge, United Kingdom and New York, NY, USA.

Katz, R.W., 1999. Extreme value theory for precipitation: sensitivity analysis for climate change. Advances in Water Resources 23, 133–139.

Katz, R.W., Brown, B.G., 1992. Extreme events in a changing climate: Variability is more important than averages. Climatic Change 21, 289–302.

Kay, A., Davies, H., Bell, V., Jones, R., 2009. Comparison of uncertainty sources for climate change impacts: flood frequency in England. Climatic Change 92, 41–63.

Kyselý, J., Beranová, R., 2008. Climate-change effects on extreme precipitation in central Europe: uncertainties of scenarios based on regional climate models. Theoretical and Applied Climatology 95, 361–374.

Li, L.J., Zhang, L., Wang, H., Wang, J., Yang, J.W., Jiang, D.J., Li, J.Y., Qin, D.Y., 2007. Assessing the impact of climate variability and human activities on streamflow from the Wuding River basin in China. Hydrological Processes 21, 3485–3491.

Li, Z., Liu, W.Z., Zhang, X.C., Zheng, F.L., 2009. Impacts of land use change and climate variability on hydrology in an agricultural catchment on the Loess Plateau of China. Journal of Hydrology 377, 35–42.

Li, Z., Zheng, F.L., Liu, W.Z., Flanagan, D.C., 2010. Spatial distribution and temporal trends of extreme temperature and precipitation events on the Loess Plateau of China during 1961–2007. Quaternary International 226, 92–100.

Li, Z., Liu, W.Z., Zhang, X.C., Zheng, F.L., 2011. Assessing the site-specific impacts of climate change on hydrology, soil erosion and crop yields in the Loess Plateau of China. Climatic Change 105, 223–242.

Lin, D., Huang, M.B., Hong, Y., 2009. Statistical Assessment of the Impact of Conservation Measures on Streamflow Responses in a Watershed of the Loess Plateau, China. Water Resources Management 23, 1935–1949.

Mearns, L.O., Katz, R.W., Schneider, S.H., 1984. Extreme high-temperature events: Changes in their probabilities with changes in mean temperature. Journal of Climate and Applied Meteorology 23, 1601–1613.

Mearns, L.O., Rosenzweig, C., Goldberg, R., 1997. Mean and variance change in climate scenarios: methods, agricultural applications, and measures of uncertainty. Climatic Change 35, 367–396.

Mu, X.M., Zhang, L., McVicar, T.R., Basang, C., Gau, P., 2007. Analysis of the impact of conservation measures on stream flow regime in catchments of the Loess Plateau, China. Hydrological Processes 21, 2124–2134.

Olesen, J., Carter, T., Díaz-Ambrona, C., Fronzek, S., Heidmann, T., Hickler, T., Holt, T., Minguez, M., Morales, P., Palutikof, J., Quemada, M., Ruiz-Ramos, M., Rubæk, G., Sau, F., Smith, B., Sykes, M., 2007. Uncertainties in projected impacts of climate change on European agriculture and terrestrial ecosystems based on scenarios from regional climate models. Climatic Change 81, 123–143.

Prudhomme, C., Davies, H., 2009. Assessing uncertainties in climate change impact analyses on the river flow regimes in the UK. Part 1: baseline climate. Climatic Change 93, 177–195.

Shan, L., 1994. Water use efficiency of plant and water utilization of agriculture in semi-arid areas. Plant Physiology Communications 30, 61–66.

Taye, M.T., Ntegeka, V., Ogiramoi, N.P., Willems, P., 2011. Assessment of climate change impact on hydrological extremes in two source regions of the Nile River Basin. Hydrology and Earth System Sciences 15, 209–222.

Thompson, L.M., 1975. Weather variability, climatic change, and grain production. Science 188, 535–541.

Wang, F.T., Liu, W.Q., 2003. Prelim inary Study of Climate Vulnerability of Agro-Production in the Loess Plateau. Climatic and Environmental Research 8, 91–100.

Wang, Y.Q., Zhou, L., 2005. Observed trends in extreme precipitation events in China during 1961–2001 and the associated changes in large-scale circulation. Geophysical Research Letters 32. doi:10.1029/2005GL022574.
Wilby, R.L., Hassan, H., Hanaki, K., 1998. Statistical downscaling of hydrometeorological variables using general circulation model output. Journal of Hydrology 205, 1–19.
Xu, J.X., 2004. Recent tendency of sediment reduction in the middle Yellow River and some countermeasures. Journal of Sediment Research 2, 5–10.
Xu, Z.X., Li, J.Y., Liu, C.M., 2007. Long-term trend analysis for major climate variables in the Yellow River basin. Hydrological Processes 21, 1935–1948.
Xu, Y., Xu, C., Gao, X., Luo, Y., 2009. Projected changes in temperature and precipitation extremes over the Yangtze River Basin of China in the 21st century. Quaternary International 208, 44–52.
Yang, S.P., Zhao, G.P., Mu, J.H., Su, Z.S., Ma, L.W., Chen, X.J., 2008. Extreme climatic events and its effect in Ningxia. Journal of Desert Research 28, 1169–1173.
Zhang, X.C., 2005. Spatial downscaling of global climate model output for site-specific assessment of crop production and soil erosion. Agricultural and Forest Meteorology 135, 215–229.
Zhang, X.P., Zhang, L., Zhao, J., Rustomji, P., Hairsine, P., 2008. Responses of streamflow to changes in climate and land use/cover in the Loess Plateau, China. Water Resources Research 44. doi:10.1029/2007wr006711.
Zhou, P.H., Wang, Z.L., 1992. A study on rainstorm causing soil erosion in the Loess Plateau. Journal of Soil and Water Conservation 6, 1–5.
Zhou, T., Yu, R., 2006. Twentieth-Century Surface Air Temperature over China and the Globe Simulated by Coupled Climate Models. Journal of Climate 19, 5843–5858.